# Fed-GLOSS-DP: Federated, Global Learning using Synthetic Sets with Record Level Differential Privacy

Hui-Po Wang Dingfan Chen Raouf Kerkouche Mario Fritz
CISPA Helmholtz Center for Information Security, Germany
{hui.wang, dingfan.chen, raouf.kerkouche, fritz}@cispa.de

#### Abstract

This work proposes Fed-GLOSS-DP, a novel privacy-preserving approach for federated learning. Unlike previous linear point-wise gradient-sharing schemes, such as FedAvg, our formulation enables a type of global optimization by leveraging synthetic samples received from clients. These synthetic samples, serving as loss surrogates, approximate local loss landscapes by simulating the utility of real images within a local region. We additionally introduce an approach to measure effective approximation regions reflecting the quality of the approximation. Therefore, the server can recover the global loss landscape and comprehensively optimize the model. Moreover, motivated by the emerging privacy concerns, we demonstrate that our approach seamlessly works with record-level differential privacy (DP), granting theoretical privacy guarantees for every data record on the clients. Extensive results validate the efficacy of our formulation on various datasets with highly skewed distributions. Our method consistently improves over the baselines, especially considering highly skewed distributions and noisy gradients due to DP. The source code will be released upon publication.

# 1 Introduction

Federated Learning (FL) [27] is a distributed learning framework that allows participants to train a model collaboratively without sharing their data. Predominantly, existing work [27, 13, 23] achieves this by training local models on clients' private datasets and sharing only the gradients with the central server. Despite extensive research over the past few years, these prevalent gradient-based methods still suffer from several challenges [12], such as data heterogeneity, potential risks of privacy breaches, and high communication costs.

Data heterogeneity [11, 24, 13] often hurts performance and convergence speed since the local updates based on the private datasets optimize the models for their local minima but suboptimal to the global objective. In this work, we propose Fed-GLOSS-DP, a novel privacy-

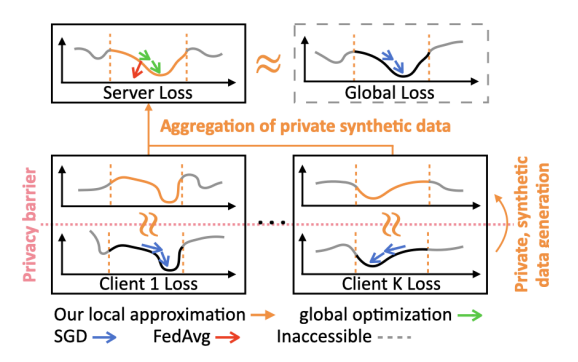


Figure 1: An overview of Fed-GLOSS-DP. It approximates local neighborhoods with synthetic images on the clients (local approximation, Sec. 4.2) and optimizes the model according to the reconstructed loss landscape on the server (global optimization, Sec. 4.3).

preserving framework that leverages synthetic images to facilitate global federated optimization. As depicted in Fig. 1, it synthesizes images to find a local approximation in the local loss landscape. These images are required to faithfully encode the information and serve as surrogates to unbiasedly communicate the essential information with the server. Meanwhile, we recognize that blindly opti-

mizing on synthetic samples could hinder performance. To address this, we present an approach that suggests a trusted region reflecting the quality of the approximation.

By aggregating the images and recognizing the effective approximation region, the central server reconstructs the global loss landscape, which is typically inaccessible in FL due to privacy constraints. This understanding allows our method to circumvent the biased update direction suggested by gradient-sharing schemes, e.g., FedAvg [27], and contributes to substantial improvements in convergence speed as demonstrated empirically in Sec. 5.

Privacy protection is another crucial aspect of FL. Although gradients are seemingly challenging to interpret, various studies have identified several threats to current federated systems, such as data leakage [10, 3, 8] and membership inference [31, 28]. These concerns motivate us to incorporate record-level differential privacy into our framework, which offers strong protection for every data record. Our method integrates seamlessly with such stringent privacy guarantees and provides reliable utility under privacy-preserving settings.

Lastly, our framework is more communication efficient as multiple optimization rounds can be performed on the server side, and – particularly for large models – transferring synthetic data is less costly than gradients in each round. Overall, we summarize our contributions as follows.

- We propose Fed-GLOSS-DP that uses synthetic images to comprehensively approach federated optimization, which has yet to be thoroughly investigated in the past.
- We demonstrate how to faithfully find local approximation and effective regions on clients, enabling efficient federated optimization on the server.
- Fed-GLOSS-DP provides rigorous record-level DP guarantees while preserving utility, surpassing gradient-sharing counterparts under privacy-preserving settings.
- Extensive experiments confirm that our formulation presents superior performance and convergence speed over existing gradient-sharing baselines, even with highly-skewed data distributions.

# 2 Related Work

**Non-IID Data in Federated Learning** causes major challenges in FL [12]. Existing efforts mainly fall into the following categories: variance-reduction techniques [13, 39], constraining the dissimilarity between clients' updates [23, 22], and adjusting the global model to a personalized version at the inference stage [26, 25, 7]. In contrast, we present a novel perspective to this challenge by resembling the global loss landscape and performing optimization from a comprehensive view.

**Dataset Distillation** Our work is largely motivated by recent progress in distilling the necessary knowledge of model training into a small set of synthetic samples [36, 42, 43, 41, 4]. Our approach is built on top of DSC [43] with several key differences. The proposed Fed-GLOSS-DP (i) focuses on finding local approximation and assembling the global loss landscape to facilitate federated optimization, (ii) is class-agnostic and complements record-level differential privacy while prior work often considers class-wise alignment and could cause privacy risks, and (iii) is designed for multi-round training with several critical design choices. The most similar work is Chen et al. [5]. They also consider class-agnostic distillation and differential privacy while focusing on one-round distillation rather than multiple-round federated learning.

#### 3 Background

#### 3.1 Federated Learning

In federated learning, we consider training a model w that maps the input x to the output prediction y. We assume K clients participate in the training, and each owns a private dataset  $\mathcal{D}_k$  with distribution  $p_k$ . We use the subscript k to represent the indices of clients, and the superscript m and t to denote the m-th communication round and t-th local step, respectively, unless stated otherwise.

Overall, the learning objective is to find the optimal model  $\mathbf{w}$  that minimizes the empirical global loss over the population distribution:

$$\mathcal{L}(\mathbf{w}) = \mathbb{E}_{(\boldsymbol{x},y) \sim p}[\ell(\mathbf{w}, \boldsymbol{x}, y)] = \frac{1}{N} \sum_{j=1}^{N} \ell(\mathbf{w}, \boldsymbol{x}_j, y_j)$$
(1)

where  $\ell$  could be arbitrary loss criteria such as cross-entropy and N is the total dataset size. However, in federated settings, direct access to the global objective is prohibited as all client data is stored locally. Instead, the optimization is conducted on local surrogate objectives  $\mathcal{L}_k(\mathbf{w})$ :

$$\mathcal{L}(\mathbf{w}) = \sum_{k=1}^K \frac{N_k}{N} \mathcal{L}_k(\mathbf{w}), \ \mathcal{L}_k(\mathbf{w}) = \sum_{j=1}^{N_k} \frac{1}{N_k} \ell(\mathbf{w}, \boldsymbol{x}_j, y_j),$$

where  $(x_j, y_j)$  are data samples from the client dataset  $\mathcal{D}_k$ .

Existing methods, such as FedAvg [27], simulate stochastic gradient descent on the global objective by performing local gradient updates and periodically aggregating and synchronizing them on the server side. Specifically, at the m-th communication round, the server broadcasts the current global model weights  $\mathbf{w}_{q}^{m,1}$  to each client, who then performs T local iterations with learning rate  $\eta$ .

$$\mathbf{w}_k^{m,1} \leftarrow \mathbf{w}_g^{m,1}, \forall k \in [K] \tag{2}$$

$$\mathbf{w}_{k}^{m,t+1} = \mathbf{w}_{k}^{m,t} - \eta \nabla \mathcal{L}_{k}(\mathbf{w}_{k}^{m,t}), \forall t \in [T]$$
(3)

The local updates  $\Delta \mathbf{w}_k^m$  are then sent back to the server and combined to construct the final global update  $g^m$ :

$$\boldsymbol{g}^{m} = \sum_{k=1}^{K} \frac{N_{k}}{N} \Delta \mathbf{w}_{k}^{m} = \sum_{k=1}^{K} \frac{N_{k}}{N} (\mathbf{w}_{k}^{m,T} - \mathbf{w}_{k}^{m,1})$$
(4)

$$\mathbf{w}_q^{m+1,1} = \mathbf{w}_q^{m,1} - \eta \mathbf{g}^m \tag{5}$$

# 3.2 Non-IID Challenges

The heterogeneity of client data distributions presents several major challenges to FL, such as a significant decrease in the convergence speed (and even divergence), and a drastic drop in the final performance when compared to the standard IID training setting [15, 23, 13, 24]. This can be easily seen from the mismatch between the local objectives that are being solved and the global objective that we are indeed aiming for, i.e.,  $\mathcal{L}_k(\mathbf{w}) \neq \mathbb{E}_{(\boldsymbol{x},y) \sim p}[\ell(\mathbf{w},\boldsymbol{x},y)]$  if  $p_k \neq p$  for some k. Executing multiple local steps on the local objective (Eq. 3) makes the local update  $\Delta \mathbf{w}_k^m$  deviate heavily from the true global gradient  $\nabla \mathcal{L}(\mathbf{w})$ , inevitably resulting in a biased approximation of the global gradient via Eq. 4 (See Fig. 1 for a demonstration.).

Despite significant advances achieved by existing works in alleviating divergence issues, these methods still exhibit bias towards optimizing the global objective as they rely on the submitted client updates  $\Delta \mathbf{w}_k^m$ , which only indicate the direction towards the client's local optimum. In contrast, our method communicates the synthetic samples  $\mathcal{S}_k$  that encode the local optimization landscapes, i.e., gradient directions within a trust region around the starting point and summarize on possible trajectories  $(\mathbf{w}_k^{m,1}, \mathbf{w}_k^{m,2}, ..., \mathbf{w}_k^{m,T+1})$ , as opposed to existing methods that communicate a single direction  $\Delta \mathbf{w}_k^m = \mathbf{w}_k^{m,T+1} - \mathbf{w}_k^{m,1}$ . This fundamental change provides the central server with a global perspective that more faithfully approximates the ground-truth global optimization (See Fig. 1 top row) than existing approaches. Moreover, unlike previous work that needs to sacrifice communication efficiency for [39] transmitting extra information (e.g., momentum) about local optimization, our approach even improves the communication efficiency by condensing the information into a small set of representative samples, with the total dimension  $\dim(\mathcal{S}_k) \ll \dim(\Delta \mathbf{w}_k^m)$ .

#### 3.3 Differential Privacy

Differential Privacy (DP) provides theoretical guarantees of privacy protection while allowing for quantitative measurement of utility. We review several definitions used in this work in this section.

**Definition 3.1** (Differential Privacy [6]). A randomized mechanism  $\mathcal{M}$  with range  $\mathcal{R}$  satisfies  $(\varepsilon, \delta)$ -DP, if for any two adjacent datasets E and E', i.e.,  $E' = E \cup \{x\}$  for some x in the data domain (or vice versa), and for any subset of outputs  $O \subseteq \mathcal{R}$ , it holds that

$$\Pr[\mathcal{M}(E) \in O] \le e^{\varepsilon} \Pr[\mathcal{M}(E') \in O] + \delta \tag{6}$$

Intuitively, DP guarantees that an adversary, provided with the output of  $\mathcal{M}$ , can only make nearly identical conclusions (within an  $\varepsilon$  margin with probability greater than  $1 - \delta$ ) about any specific

record, regardless of whether it was included in the input of  $\mathcal{M}$  or not [6]. This suggests that, for any record owner, a privacy breach due to its participation in the dataset is unlikely.

In FL, the notion of *adjacent* (*neighboring*) datasets used in DP generally refers to pairs of datasets differing by either one user (*user-level* DP) or a single data point of one user (*record-level* DP). Our work focuses on the latter. While there are established methods providing record-level DP for training federated models [34, 32, 14], these primarily operate on the transmitted single client gradients, adhering to traditional (non-private) FL methodologies. In contrast, our novel formulation allows efficient communication of comprehensive information about the local loss landscape, thereby facilitating global optimization and displaying improved training stability and utility.

We use the Gaussian mechanism to upper bound privacy leakage when transmitting information from clients to the server.

**Definition 3.2.** (Gaussian Mechanism [6]) Let  $f: \mathbb{R}^n \to \mathbb{R}^d$  be an arbitrary function with sensitivity being the maximum Euclidean distance between the outputs over all adjacent datasets E and  $E' \in \mathcal{E}$ :

$$\Delta_2 f = \max_{E, E'} \| f(E) - f(E') \|_2 \tag{7}$$

The Gaussian Mechanism  $\mathcal{M}_{\sigma}$ , parameterized by  $\sigma$ , adds noise into the output, i.e.,

$$\mathcal{M}_{\sigma}(\mathbf{x}) = f(\mathbf{x}) + \mathcal{N}(0, \sigma^{2}\mathbb{I}). \tag{8}$$

$$\mathcal{M}_{\sigma}$$
 is  $(\varepsilon, \delta)$ -DP for  $\sigma \geq \sqrt{2 \ln (1.25/\delta)} \Delta_2 f/\varepsilon$ .

Moreover, we use the following theorem to guarantee that the privacy leakage is bounded upon obtaining gradients from real private data in our framework. This forms the basis for the overall privacy guarantee of our framework and enables us to enhance the approximation quality without introducing additional privacy costs.

**Theorem 3.3.** (Post-processing [6]) If  $\mathcal{M}$  satisfies  $(\varepsilon, \delta)$ -DP,  $G \circ \mathcal{M}$  will satisfy  $(\varepsilon, \delta)$ -DP for any data-independent function G.

# 4 Fed-GLOSS-DP: Federated, Global Learning using Synthetic Sets

#### 4.1 Overview

**Setting.** We focus on the conventional FL setting in which each client retains their private data locally, and the local data cannot be directly accessed by the server. Every data sample is deemed private, with neither the server nor the clients using any additional (public) data, which stands in contrast to previous works that require extra data on the server side [44, 21]. Furthermore, all clients aim towards a singular global objective (Eq. 1), which is distinct from personalized approaches wherein evaluations are conducted based on each client's unique objective and their own data distribution [25, 7, 26].

**Formulation.** Unlike existing approaches that typically communicate the local update directions to approximate the optimization of the global objective (Eq. 4), we propose to directly simulate the global optimization by transmitting a small set of synthetic samples that reflect the local loss landscapes (Fig. 1). Such synthetic data can then be leveraged by the central server as if it were the real data, allowing the training process to mimic the ground-truth global optimization as if we had access to the complete client data distribution.

Let  $p_k$  and the  $p_{S_k}$  be the distribution of the real client dataset  $\mathcal{D}_k$  and the corresponding synthetic dataset  $S_k$ , respectively. Our objective can be formalized as:

$$\mathbb{E}_{(\boldsymbol{x},y)\sim p_k}[\ell(\mathbf{w},\boldsymbol{x},y)] \simeq \mathbb{E}_{(\hat{\boldsymbol{x}},\hat{y})\sim p_{\mathcal{S}_k}}[\ell(\mathbf{w},\hat{\boldsymbol{x}},\hat{y})]$$
(9)

The server can then recover the true global objective by:

$$\mathcal{L}(\mathbf{w}) = \sum_{k=1}^{K} \frac{N_k}{N} \mathcal{L}_k(\mathbf{w}) \simeq \sum_{k=1}^{K} \frac{N_k}{N} \widehat{\mathcal{L}}_k(\mathbf{w})$$
 (10)

with  $\mathcal{L}_k(\mathbf{w})$  being the left-hand side of Eq. 9 and  $\widehat{\mathcal{L}}_k(\mathbf{w}) = \frac{1}{|S_k|} \sum_{j=1}^{|S_k|} \ell(\mathbf{w}, \hat{x}_j, \hat{y}_j)$  the right-hand side. Performing global updates is then equivalent to conducting vanilla gradient descent on the recovered global objective, i.e., by training on the synthetic set of samples.

We demonstrate our framework in Fig. 1. In every communication round, synthetic samples are optimized to approximate the client's local loss landscapes and then transmitted to the server. The server then performs global updates on the synthetic samples to simulate global optimization.

In the following, we explain how to construct the synthetic datasets on each client that encode the local loss landscapes (Sec 4.2) and how to optimize the global model over a reconstructed loss landscape on the server (Sec 4.3). Lastly, we show in Sec 4.4 that our method is seamlessly compatible with *record-level* differential privacy. The overall algorithm is depicted in Algorithm 1.

# **Algorithm 1** Fed-GLOSS

```
function ClientExecute(k, r, \mathbf{w}_a^{m,1}):
                                                                                                                Initialize S_k: \{\hat{\boldsymbol{x}}_k^m\} from Gaussian noise or \{\hat{\boldsymbol{x}}_k^{m-1}\},
function ServerExecute:
                                                                                                                \{\hat{y}_k\} to be a balanced set
    Initialize global weight \mathbf{w}_g^{1,1}, radius r
                                                                                                                for i=1,\ldots,R_i do
    /* Local approximation */
                                                                                                                    /* Resample training trajectories */
    for m=1,\ldots,M do
                                                                                                                    Reset t \leftarrow 1 and model \mathbf{w}_k^{m,1} \leftarrow \mathbf{w}_q^{m,1}
                                                                                                                    while ||\mathbf{w}_{k}^{m,t} - \mathbf{w}_{k}^{m,1}|| < r \mathbf{do}

Sample real data batches \{(\mathbf{x}_{k}, y_{k})\} from \mathcal{D}_{k}

Compute g^{\mathcal{D}} = \nabla \mathcal{L}(\mathbf{w}_{k}^{m,t}, \{(\mathbf{x}_{k}, y_{k})\})
          for k = 1, \dots, K do
               S_k, r_k \leftarrow \text{ClientsExecute}(k, r, \mathbf{w}_q^{m,1})
          /* Global optimization */
                                                                                                                         for j=1,\ldots,R_b do
          r_g \leftarrow \min\{r_k\}_{k=1}^K
                                                                                                                             /* Update synthetic set S_k */
         \tilde{t\leftarrow 1}
                                                                                                                             S_k = S_k - \tau \nabla_{S_k} \mathcal{L}_{dis} \left( g^{\mathcal{D}}, \nabla \mathcal{L}(\mathbf{w}_k^{m,t}, S_k) \right)
         \begin{aligned} & \textbf{while} \ \| \mathbf{w}_g^{m,1} - \mathbf{w}_g^{m,t} \| < r_g \ \textbf{do} \\ & \mathbf{w}_g^{m,t+1} = \mathbf{w}_g^{m,t} - \sum_{k=1}^K \eta \frac{N_k}{N} \nabla \mathcal{L}(\mathbf{w}_g^{m,t}, \mathcal{S}_k) \\ & t \leftarrow t+1 \end{aligned}
                                                                                                                         for l=1,\ldots,R_l do
                                                                                                                             /* Update local model parameter \mathbf{w}_k */
                                                                                                                             \mathbf{w}_{k}^{m,t+1} = \mathbf{w}_{k}^{m,t} - \eta \nabla \mathcal{L}(\mathbf{w}_{k}^{m,t}, \mathcal{S}_{k})
          end while
         \mathbf{w}_q^{m+1,1} \leftarrow \mathbf{w}_g^{m,t}
                                                                                                                         end for
     end for
                                                                                                                    end while
Return: global model weight \mathbf{w}_{q}^{M+1,1}
                                                                                                                Measure r_k on \mathcal{D}_k (See Fig. 2)
                                                                                                            Return: Synthetic set S_k, calibrated radius r_k
```

#### 4.2 Local Approximation

The goal of this step is to construct a set of synthetic samples  $\mathcal{S}_k$  that accurately captures necessary local information for subsequent global updates. A natural approach would be to enforce similarity between the gradients obtained from the real client data and those obtained from the synthetic set:

$$\nabla_{\mathbf{w}} \mathbb{E}_{(\boldsymbol{x},y) \sim p_k} [\ell(\mathbf{w},\boldsymbol{x},y)] \simeq \nabla_{\mathbf{w}} \mathbb{E}_{(\hat{\boldsymbol{x}},\hat{y}) \sim p_{\mathcal{S}_k}} [\ell(\mathbf{w},\hat{\boldsymbol{x}},\hat{y})]$$

We achieve this by minimizing the distance between the gradients:

$$\underset{\mathcal{S}_k}{\operatorname{arg\,min}} \quad \mathcal{L}_{\operatorname{dis}}\Big(\nabla \mathcal{L}(\mathbf{w}, \mathcal{D}_k), \nabla \mathcal{L}(\mathbf{w}, \mathcal{S}_k)\Big) \quad (11)$$

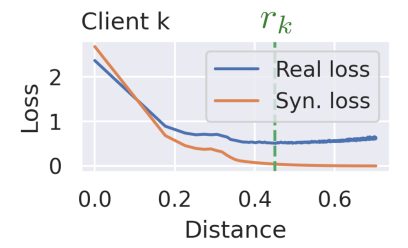


Figure 2:  $r_k$  selection. The losses on private real and synthetic data decrease initially but deviate later.  $r_k$  is defined as the turning points with the smallest real loss.

where we denote  $\nabla \mathcal{L}(\mathbf{w}, \mathcal{D}_k)$ ) the stochastic gradient of network parameters on the client dataset  $\mathcal{D}_k$ , and  $\nabla \mathcal{L}(\mathbf{w}, \mathcal{S}_k)$  the gradient on the synthetic set for brevity. Following existing literature [42, 43], we adopt for  $\mathcal{L}_{dis}$  a layer-wised cosine distance coupled with a mean square error term to encode the directional information of the gradients and to regulate the discrepancy in their magnitude, which we found critical for multi-round training. (See appendix for more details).

While solving Eq. 11 for every possible w would lead to perfect recovery of the ground-truth global optimization in principle, in practice, however, it is infeasible due to the large space of (infinitely many) possible values of w. Additionally, as  $|S_K|$  is set to be much smaller than  $N_k$  (for the sake of communication efficiency), an exact solution may not exist, resulting in approximation error for some w. To address this, we explicitly constrain the problem space to be the most achievable region for further global updates. Specifically, we consider  $w_k$  that is sufficiently close to the initial point of

the local update and is located on the update trajectories (Eq. 13). Formally,

$$\underset{\mathcal{S}_k}{\operatorname{arg\,min}} \sum_{t=1}^{T} \mathcal{L}_{\operatorname{dis}} \Big( \nabla \mathcal{L}(\mathbf{w}_k^{m,t}, \mathcal{D}_k), \nabla \mathcal{L}(\mathbf{w}_k^{m,t}, \mathcal{S}_k) \Big)$$
(12)

s.t. 
$$\|\mathbf{w}_k^{m,t} - \mathbf{w}_k^{m,1}\| < r$$
 and  $\mathbf{w}_k^{m,t+1} = \mathbf{w}_k^{m,t} - \eta \nabla \mathcal{L}(\mathbf{w}_k^{m,t}, \mathcal{S}_k)$  (13)

In the m-th communication round, the clients first synchronize the local model  $\mathbf{w}_k^{m,1}$  with the global model  $\mathbf{w}_g^{m,1}$  and initialize the synthetic features  $\{\hat{\mathbf{x}}_k^m\}$  either from Gaussian noise or to be the ones obtained from the previous round  $\{\hat{\mathbf{x}}_k^{m-1}\}$ . Synthetic labels  $\{\hat{y}_k\}$  are initialized to be a fixed, balanced set and are not optimized during the training process. The number of synthetic samples  $|\mathcal{S}_k|$  is kept equal for all clients in our experiments, though it can be adjusted for each client depending on factors such as local dataset size and bandwidth in practice.

To simulate the local training trajectories, the clients alternate between updating synthetic features (by performing gradient descent of Eq. 12 w.r.t.  $\hat{\mathbf{x}}_k$ ) and updating the local model using Eq. 13. This process continues until the current local model weight  $\mathbf{w}_k^{m,t}$  exceeds the trust region, meaning it is no longer close to the initial point. This is determined by whether the Euclidean distance on the flattened weight vectors exceeds a predefined radius r. Additionally, an appropriate radius r should reflect the overall training progress and the client's training status, e.g., it should decrease when the global training is close to convergence and should be small for some clients with data that is hard to fit. Thus, we suggest calibrating the radius based on the training progress at each client, as illustrated in Fig. 2. For the DP training setting, we make the choice of  $r_k$  data-independent (See Sec. 4.4).

# 4.3 Global Optimization

Once the server received the synthetic set  $\mathcal{S}_k$  and the calibrated radius  $r_k$ , global updates can be performed by conducting gradient descent directly on the synthetic set of samples. The global objective can be recovered by  $\widehat{\mathcal{L}}_k(\mathbf{w})$  according to Eq. 10 (i.e., training on the synthetic samples), while the scaling factor  $\frac{N_k}{N}$  can be treated as the scaling factor of the learning rate when computing the gradients on samples from each synthetic set  $\mathcal{S}_k$ , namely:

$$\mathbf{w}_g^{m,t+1} = \mathbf{w}_g^{m,t} - \sum_{k=1}^K \eta \cdot \frac{N_k}{N} \nabla_{\mathbf{w}} \mathcal{L}(\mathbf{w}_g^{m,t}, \mathcal{S}_k)$$
 (14)

s.t. 
$$\|\mathbf{w}_g^{m,t} - \mathbf{w}_g^{m,1}\| \le \min\{r_k\}_{k=1}^K$$
 (15)

The constraint in Eq. 15 enforces that the global update respect the vicinity suggested by the clients, meaning updates are only made within regions where the approximation is sufficiently accurate.

#### 4.4 Record-level DP

While federated systems offer a basic level of privacy protection by keeping client data local, we further address possible privacy concerns that might arise during the transfer of synthetic data in our proposed method. Specifically, we rigorously limit privacy leakage by integrating record-level DP, a privacy notion widely used in FL applications. This is especially important in cross-silo scenarios, such as collaborations between hospitals, where each institution acts as a client, aiming to train a predictive model and leveraging patient data with varying distributions across different hospitals while ensuring strict privacy protection for patients.

**Threat model.** In a federated system, there can be one or multiple colluding adversaries who have access to update vectors from any party during each communication round. These adversaries may have unlimited computation power but remain passive or "honest-but-curious," meaning they follow the learning protocol faithfully without modifying any update vectors [34, 32, 14]. These adversaries can represent any party involved, such as a malicious client or server, aiming to extract information from other parties. The central server possesses knowledge of label classes for each client's data, while clients may or may not know the label classes of other clients' data. While we typically do not intentionally hide label class information among clients, our approach is flexible and can handle scenarios where clients want to keep their label class information confidential from others.

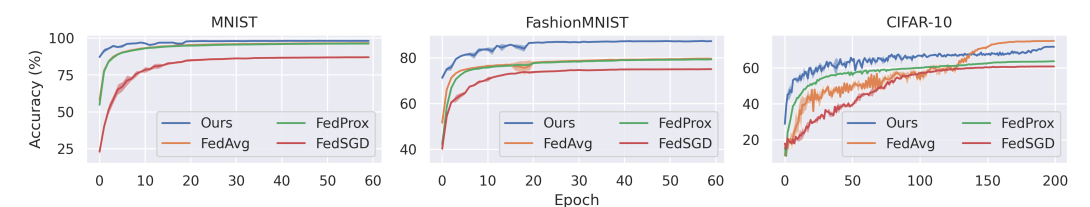


Figure 3: Accuracy over communication rounds with extremely non-IID data.

**Operation.** We integrate record-level DP into Fed-GLOSS to provide theoretical privacy guarantees, which yields Fed-GLOSS-DP. Given a desired privacy budget  $(\varepsilon, \delta)$ , we sanitize the gradients derived from real data with the Gaussian mechanism, denoted by  $\nabla \widetilde{\mathcal{L}}(\mathbf{w}_k^{m,t}, \mathcal{D}_k)$ . The DP-guaranteed local approximation can be realized by replacing the learning target of Eq. 12 with the sanitized gradients while leaving other constraints the same. Formally, we have

$$\underset{\mathcal{S}_{k}}{\operatorname{arg\,min}} \sum_{t=1}^{T} \mathcal{L}_{\operatorname{dis}} \Big( \nabla \widetilde{\mathcal{L}}(\mathbf{w}_{k}^{m,t}, \mathcal{D}_{k}), \nabla \mathcal{L}(\mathbf{w}_{k}^{m,t}, \mathcal{S}_{k}) \Big) 
\text{s.t.} \quad \|\mathbf{w}_{k}^{m,t} - \mathbf{w}_{k}^{m,1}\| < r \quad \text{and} \quad \mathbf{w}_{k}^{m,t+1} = \mathbf{w}_{k}^{m,t} - \eta \nabla \mathcal{L}(\mathbf{w}_{k}^{m,t}, \mathcal{S}_{k})$$
(16)

We elaborate on the process of generating sanitized gradients and present the privacy analysis of Fed-GLOSS-DP in the Appendix. Notably, our work distinguishes itself from existing work on centralized DP data synthesis [5] in two main aspects. Firstly, in contrast to the existing single-shot distillation approach, our method is specifically designed for multiple-round training by approximating the loss surface in an r neighborhood around the current local parameter  $\mathbf{w}_k^{m,t}$ . Secondly, we take advantage of Theorem 3.3 by designing an extra iteration  $R_b$  over the updates of the synthetic set  $\mathcal{S}_k$  to enhance approximation quality without introducing additional privacy costs.

# 5 Experiments

#### 5.1 Setup

We consider a standard classification task by training federated ConvNets [20] on three benchmark datasets: MNIST [19], FashionMNIST [38], and CIFAR-10 [17]. Our study focuses on the non-IID setting where five clients possess disjoint class sets, meaning each client holds two unique classes. This scenario is typically considered challenging [11] and mirrors the cross-silo setting [12] where all clients participate in every training round while maintaining a relatively large amount of data, yet exhibiting statistical divergence (e.g., envision the practical scenario for collaborations among hospitals). Our method employs a learning rate of 100 for updating synthetic images and 0.1 with cosine decay for model updates. We set by default  $(R_i, R_l, R_b, r) = (4, 2, 10, 1.5)$  and (1, 0, 5, 10) for the DP and non-DP training, respectively. To prevent infinite loops caused by the neighborhood search, we upper bound the while loops in Algorithm 1 by 5 iterations. We follow FL benchmarks [27, 33] and the official codes for training the baselines. All experiments are repeated over three random seeds. More details are provided in Appendix.

#### 5.2 Data Heterogeneity

	DSC <sup>†</sup> [42]	FedSGD [27]	FedAvg [27]	FedProx [23]	SCAFFOLD [1	[3] Ours
		(1×)	$(1\times)$	$(1\times)$	$(2\times)$	$(0.96\times)$
MNIST	98.90±0.20	87.07±0.65	96.55±0.21	96.26±0.04	97.56±0.06	98.08±0.02
FashionMNIST	83.60±0.40	75.10±0.16	79.67±0.56	79.37±0.29	82.17±0.37	87.37±0.09
CIFAR-10	53.90±0.50	60.91±0.19	$75.20\pm0.12$	63.84±0.45	56.27±1.19	71.91±0.20

Table 1: Performance comparison on benchmark datasets. The relative communication cost of each method (w.r.t. the model size) is shown in brackets. DSC<sup>†</sup> is ported from the original paper and conducted in a one-shot centralized setting.

We first demonstrate the effectiveness of Fed-GLOSS over various baselines on benchmark datasets in a non-IID setting. Our method assigns 50 images to each class, resulting in comparable communication costs to the baselines. The baselines include: **DSC** [42], the dataset distillation method

	PSG <sup>†</sup> [5]	DP-FedAvg	DP-FedProx	Ours	DP-FedAvg	DP-FedProx	Ours
ε	32		2.79			10.18	
MNIST	88.34±0.8	45.25±6.9	54.58±4.9	60.72±1.3	86.99±0.5	88.75±0.5	87.77±0.8
FMNIST	67.91±0.3	50.11±4.2	54.57±2.9	59.85±1.5	72.78±1.3	71.67±2.2	$73.00\pm0.7$
CIFAR-10	34.58±0.4	17.11±0.7	19.40±0.7	21.42±1.4	31.15±0.4	35.04±1.1	36.09±0.5

Table 2: Utility and Privacy budgets at varying privacy regimes. The high privacy regime with  $\varepsilon=2.79$  corresponds to the first communication round, while a privacy level of  $\varepsilon=10.18$  represents the commonly considered point ( $\varepsilon=10$ ) in private learning literature. PSG<sup>†</sup> corresponds to a one-shot setting and is reproduced from the official code.

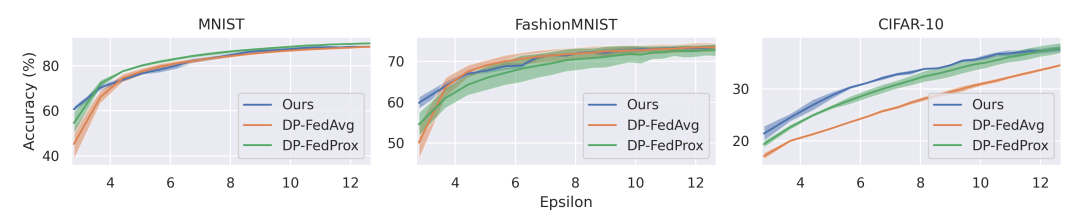


Figure 4: Privacy-utility trade-off with  $\delta = 10^{-5}$ . A *smaller* value of  $\varepsilon$  (x-axis) indicates a *stronger* privacy guarantee. Evaluation is conducted at each communication round.

algorithmically most similar to ours; **FedSGD** [27], that transmits every single batch gradient to prevent potential model drifting; **FedAvg** [27], the most representative FL method; **FedProx** [23] and **SCAFFOLD** [13], state-of-the-art federated optimization for non-IID distributions. Note that DSC operates in a (one-shot) centralized setting, and SCAFFOLD incurs double the communication costs compared to the others by design. As depicted in Table 1, our method surpasses DSC and FedSGD, highlighting the benefits of multi-round training on the server and client sides, respectively. Moreover, our method presents superior performance over state-of-the-art optimization methods, validating the strength of optimizing from a global view. We also plot model utility against training rounds in Fig. 3, where our method consistently exhibits the fastest convergence across all three datasets. In other words, our methods consume fewer costs to achieve the same or better performance level and thus more communication efficient.

# 5.3 Privacy Protection

We evaluate the trade-off between utility and privacy costs  $\varepsilon$  on benchmark datasets against two state-of-the-art methods, **DP-FedAvg** [34] and **DP-FedProx**. Our method assigns 10 images per class and is evaluated under the worst-case scenario, i.e., we assume the maximum of 5 while loops is always reached (Sec. 5.1) for the  $\varepsilon$  computation, despite the potential early termination (and thus smaller  $\varepsilon$ ) caused by the radius r (Eq. 13). To ensure a fair and transparent comparison, we require our method to access the same amount of private data as the baselines in every communication round and consider a noise scale  $\sigma=1$  for all approaches. Fig. 4 demonstrates that our framework generally exhibits superior performance, notably with smaller  $\varepsilon$  and more complex datasets such as CIFAR-10. This superiority is further quantified in Table 2 under two typical privacy budgets of 2.79 and 10.18. Moreover, when compared to the private one-shot dataset condensation method (**PSG** [5]), our approach presents a better privacy-utility trade-off, effectively leveraging the benefits of multi-round training in the challenging federated setting.

### 5.4 Ablation Study

**Radius Selection.** As in Sec. 4, we evaluate different radius selection strategies for server optimization. We consider four strategies: *Fixed*, *Max*, *Median*, and *Min*. *Fixed* uses a fixed length

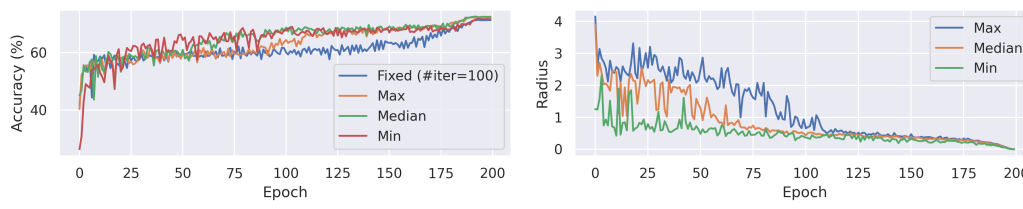


Figure 5: Ablation study on radius selection.

Figure 6: Radius suggested by different strategies.

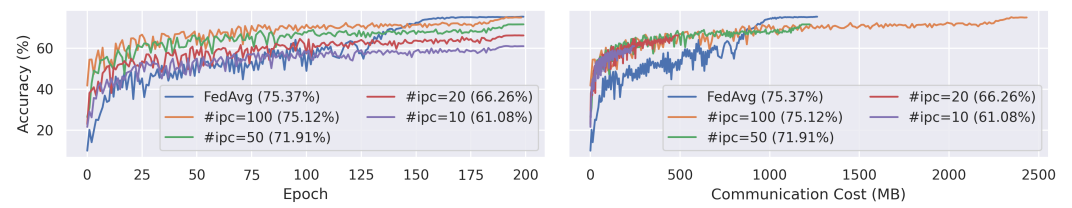


Figure 7: Ablation study on the number of images per class (#ipc).

of 100 iterations, ignoring the quality. *Max* aims for the fastest optimization by using the largest radius. *Median* optimizes in a moderate way by considering the majority. *Min*, adopted in all experiments, focuses on the safest region agreed upon by all synthetic image sets. Table 3 reveals that the proposed strategies consistently outperform the fixed strategy. Meanwhile, Fig. 5 presents that a more aggressive strategy leads to worse intermediate performance, which may not be suitable for federated applications requiring satisfactory intermediate performance. Among them, *Min* delivers the best results. Finally, Fig. 6 demonstrates that the radii proposed by different strategies change across epochs, indicating that a naively set training iteration may not be optimal. Additionally, this finding suggests the possibility of designing heuristic scheduling functions for adjusting the radius in a privacy-preserving way. The corresponding server training iterations can be found in the appendix.

**Size of synthetic datasets.** We investigate the impact of synthetic dataset size on approximation. In general, higher numbers of synthetic samples submitted by clients lead to greater information communication. To further explore this concept, we conducted experiments on CIFAR-10, building

Min	Max	Median	Fixed			
71.90	72.39	72.33	71.26			
Table 3: Performance comparison be-						
tween the radius selection strategies.						

upon the previous experiment (shown in Fig. 3) by adding three additional settings in which we assigned 10, 20, and 100 images to each class (referred to as "image per class" or #ipc). Our results, presented in Fig. 7, demonstrate that our method performs best when assigning 100 images, supporting the hypothesis that more synthetic samples convey more information. Additionally, our method produces superior outcomes regardless of #ipc when communication costs are restricted, making it advantageous for resource-constrained devices.

# 6 Discussion

**Future directions.** While the primary contribution of Fed-GLOSS lies in utilizing local approximation for global optimization, we demonstrate in the appendix that its performance can be further enhanced by improving the quality of the approximation. Moreover, ongoing research in synthetic data generation [43, 41, 4] represents a potential avenue for future work, which could potentially benefit our formulation.

**Privacy and auditing.** While there exists a conflict between privacy and auditing in federated learning, Fed-GLOSS-DP provides a potential solution for reconciling these two aspects. In the appendix, we visualize the synthetic samples and corresponding pixel distributions, highlighting the variations in statistics between the clients and the server across different training rounds and parties. These observations present an opportunity to develop privacy-preserving approaches for auditing FL.

# 7 Conclusion

In conclusion, this work introduces Fed-GLOSS-DP, a novel approach for privacy-preserving federated learning. Fed-GLOSS-DP utilizes synthetic data to encode the local loss landscape within calibrated trust regions, effectively debiasing the optimization by the server. Moreover, our method seamlessly integrates record-level differential privacy, thereby ensuring strict privacy protection for individual data records. Extensive experimental results demonstrate that Fed-GLOSS-DP outperforms gradient-sharing approaches in terms of faster convergence on highly-skewed data splits and reliable utility under differential privacy settings. We further explore the critical role of radius selection, the influence of synthetic dataset size, and potential enhancements to our framework. Overall, Fed-GLOSS-DP presents a promising approach for privacy-preserving federated learning, addressing the challenges of convergence stability and privacy protection in non-IID scenarios.

# Acknowledgment

This work was partially funded by the Helmholtz Association within the project "Trustworthy Federated Data Analytics (TFDA)" (ZT-I-OO1 4), ELSA, privateAIM, and priSyn.

# References

- [1] M. Abadi, A. Chu, I. Goodfellow, H. B. McMahan, I. Mironov, K. Talwar, and L. Zhang. Deep learning with differential privacy. In *Proceedings of the 2016 ACM SIGSAC conference on computer and communications security*, pages 308–318, 2016.
- [2] B. Balle, G. Barthe, M. Gaboardi, J. Hsu, and T. Sato. Hypothesis testing interpretations and renyi differential privacy. In *International Conference on Artificial Intelligence and Statistics*, pages 2496–2506. PMLR, 2020.
- [3] A. Bhowmick, J. Duchi, J. Freudiger, G. Kapoor, and R. Rogers. Protection against reconstruction and its applications in private federated learning. *arXiv preprint arXiv:1812.00984*, 2018.
- [4] G. Cazenavette, T. Wang, A. Torralba, A. A. Efros, and J.-Y. Zhu. Dataset distillation by matching training trajectories. In *Proceedings of the IEEE Conference on Computer Vision and Pattern Recognition (CVPR)*, pages 4750–4759, 2022.
- [5] D. Chen, R. Kerkouche, and M. Fritz. Private set generation with discriminative information. In *Advances in Neural Information Processing Systems (NeurIPS)*, 2022.
- [6] C. Dwork, A. Roth, et al. The algorithmic foundations of differential privacy. *Foundations and Trends® in Theoretical Computer Science*, 9(3–4):211–407, 2014.
- [7] A. Fallah, A. Mokhtari, and A. Ozdaglar. Personalized federated learning with theoretical guarantees: A model-agnostic meta-learning approach. *Advances in Neural Information Processing Systems (NeurIPS)*, 33:3557–3568, 2020.
- [8] J. Geiping, H. Bauermeister, H. Dröge, and M. Moeller. Inverting gradients-how easy is it to break privacy in federated learning? *Advances in Neural Information Processing Systems* (*NeurIPS*), 33:16937–16947, 2020.
- [9] Y. He, H.-P. Wang, M. Zenk, and M. Fritz. Cossgd: Communication-efficient federated learning with a simple cosine-based quantization. *arXiv preprint arXiv:2012.08241*, 2020.
- [10] B. Hitaj, G. Ateniese, and F. Perez-Cruz. Deep models under the gan: information leakage from collaborative deep learning. In *Proceedings of the 2017 ACM SIGSAC conference on computer* and communications security, pages 603–618, 2017.
- [11] T.-M. H. Hsu, H. Qi, and M. Brown. Measuring the effects of non-identical data distribution for federated visual classification. *arXiv* preprint arXiv:1909.06335, 2019.
- [12] P. Kairouz, H. B. McMahan, B. Avent, A. Bellet, M. Bennis, A. N. Bhagoji, K. Bonawitz, Z. Charles, G. Cormode, R. Cummings, et al. Advances and open problems in federated learning. *Foundations and Trends*® *in Machine Learning*, 14(1–2):1–210, 2021.
- [13] S. P. Karimireddy, S. Kale, M. Mohri, S. Reddi, S. Stich, and A. T. Suresh. Scaffold: Stochastic controlled averaging for federated learning. In *Proceedings of the International Conference on Machine Learning (ICML)*. PMLR, 2020.
- [14] R. Kerkouche, G. Acs, C. Castelluccia, and P. Genevès. Privacy-preserving and bandwidth-efficient federated learning: An application to in-hospital mortality prediction. In *Proceedings of the Conference on Health, Inference, and Learning*, pages 25–35, 2021.
- [15] A. Khaled, K. Mishchenko, and P. Richtárik. First analysis of local gd on heterogeneous data. *arXiv preprint arXiv:1909.04715*, 2019.
- [16] M. Khodak, R. Tu, T. Li, L. Li, M.-F. F. Balcan, V. Smith, and A. Talwalkar. Federated hyperparameter tuning: Challenges, baselines, and connections to weight-sharing. *Advances in Neural Information Processing Systems*, 34:19184–19197, 2021.

- [17] A. Krizhevsky, G. Hinton, et al. Learning multiple layers of features from tiny images. 2009.
- [18] A. Kurakin, S. Song, S. Chien, R. Geambasu, A. Terzis, and A. Thakurta. Toward training at imagenet scale with differential privacy. *arXiv preprint arXiv:2201.12328*, 2022.
- [19] Y. LeCun, L. Bottou, Y. Bengio, and P. Haffner. Gradient-based learning applied to document recognition. *Proceedings of the IEEE*, 86(11):2278–2324, 1998.
- [20] Y. LeCun, K. Kavukcuoglu, and C. Farabet. Convolutional networks and applications in vision. In *Proceedings of 2010 IEEE international symposium on circuits and systems*, pages 253–256. IEEE, 2010.
- [21] D. Li and J. Wang. Fedmd: Heterogenous federated learning via model distillation. arXiv preprint arXiv:1910.03581, 2019.
- [22] Q. Li, B. He, and D. Song. Model-contrastive federated learning. In *Proceedings of the IEEE/CVF Conference on Computer Vision and Pattern Recognition*, pages 10713–10722, 2021.
- [23] T. Li, A. K. Sahu, M. Zaheer, M. Sanjabi, A. Talwalkar, and V. Smith. Federated optimization in heterogeneous networks. *Proceedings of Machine Learning and Systems*, 2020.
- [24] X. Li, K. Huang, W. Yang, S. Wang, and Z. Zhang. On the convergence of fedavg on non-iid data. *arXiv preprint arXiv:1907.02189*, 2019.
- [25] X. Li, M. JIANG, X. Zhang, M. Kamp, and Q. Dou. Fedbn: Federated learning on non-iid features via local batch normalization. In *Proceedings of the International Conference on Learning Representations (ICLR)*, 2021.
- [26] M. Luo, F. Chen, D. Hu, Y. Zhang, J. Liang, and J. Feng. No fear of heterogeneity: Classifier calibration for federated learning with non-iid data. *Advances in Neural Information Processing Systems*, 34, 2021.
- [27] B. McMahan, E. Moore, D. Ramage, S. Hampson, and B. A. y Arcas. Communication-efficient learning of deep networks from decentralized data. In *Proceedings of the International Conference on Artificial Intelligence and Statistics (AISTATS)*, pages 1273–1282. PMLR, 2017.
- [28] L. Melis, C. Song, E. De Cristofaro, and V. Shmatikov. Exploiting unintended feature leakage in collaborative learning. In *2019 IEEE symposium on security and privacy (SP)*, pages 691–706. IEEE, 2019.
- [29] I. Mironov. Rényi differential privacy. In 2017 IEEE 30th computer security foundations symposium (CSF), pages 263–275. IEEE, 2017.
- [30] I. Mironov, K. Talwar, and L. Zhang. R\'enyi differential privacy of the sampled gaussian mechanism. *arXiv preprint arXiv:1908.10530*, 2019.
- [31] M. Nasr, R. Shokri, and A. Houmansadr. Comprehensive privacy analysis of deep learning: Passive and active white-box inference attacks against centralized and federated learning. In 2019 IEEE symposium on security and privacy (SP), pages 739–753. IEEE, 2019.
- [32] D. Peterson, P. Kanani, and V. J. Marathe. Private federated learning with domain adaptation. arXiv preprint arXiv:1912.06733, 2019.
- [33] S. J. Reddi, Z. Charles, M. Zaheer, Z. Garrett, K. Rush, J. Konečný, S. Kumar, and H. B. McMahan. Adaptive federated optimization. In *International Conference on Learning Representations (ICLR)*, 2021.
- [34] S. Truex, N. Baracaldo, A. Anwar, T. Steinke, H. Ludwig, R. Zhang, and Y. Zhou. A hybrid approach to privacy-preserving federated learning. In *Proceedings of the 12th ACM workshop on artificial intelligence and security*, 2019.
- [35] H.-P. Wang, S. Stich, Y. He, and M. Fritz. Progfed: effective, communication, and computation efficient federated learning by progressive training. In *Proceedings of the International Conference on Machine Learning (ICML)*, pages 23034–23054. PMLR, 2022.

- [36] T. Wang, J.-Y. Zhu, A. Torralba, and A. A. Efros. Dataset distillation. arXiv preprint arXiv:1811.10959, 2018.
- [37] Y. Wu and K. He. Group normalization. In *Proceedings of the European conference on computer vision (ECCV)*, pages 3–19, 2018.
- [38] H. Xiao, K. Rasul, and R. Vollgraf. Fashion-mnist: a novel image dataset for benchmarking machine learning algorithms. *arXiv preprint arXiv:1708.07747*, 2017.
- [39] H. Yu, R. Jin, and S. Yang. On the linear speedup analysis of communication efficient momentum sgd for distributed non-convex optimization. In *International Conference on Machine Learning*. PMLR, 2019.
- [40] B. Zhao and H. Bilen. Dataset condensation with differentiable siamese augmentation. In *Proceedings of the International Conference on Machine Learning (ICML)*, pages 12674–12685. PMLR, 2021.
- [41] B. Zhao and H. Bilen. Dataset condensation with distribution matching. In *Proceedings of the IEEE/CVF Winter Conference on Applications of Computer Vision*, pages 6514–6523, 2023.
- [42] B. Zhao, K. R. Mopuri, and H. Bilen. Dataset condensation with gradient matching. arXiv preprint arXiv:2006.05929, 2020.
- [43] B. Zhao, K. R. Mopuri, and H. Bilen. Dataset condensation with gradient matching. In *Proceedings of the International Conference on Learning Representations (ICLR)*, 2021.
- [44] Y. Zhao, M. Li, L. Lai, N. Suda, D. Civin, and V. Chandra. Federated learning with non-iid data. *arXiv preprint arXiv:1806.00582*, 2018.

# **Appendix**

# A Privacy Analysis

#### A.1 Definitions

**Definition A.1** (Rényi divergence). Let P and Q be two distributions defined over the same probability space  $\mathcal{X}$ . Let their respective densities be denoted as p and q. The Rényi divergence, of a finite order  $\alpha \neq 1$ , between the distributions P and Q is defined as follows:

$$D_{\alpha}(P \parallel Q) \stackrel{\Delta}{=} \frac{1}{\alpha - 1} \ln \int_{\mathcal{X}} q(x) \left( \frac{p(x)}{q(x)} \right)^{\alpha} dx$$
.

Rényi divergence at orders  $\alpha = 1, \infty$  are defined by continuity.

**Definition A.2** (Rényi differential privacy (RDP) [29]). A randomized mechanism  $\mathcal{M}: \mathcal{E} \to \mathcal{R}$  satisfies  $(\alpha, \rho)$ -Rényi differential privacy (RDP) if for any two adjacent inputs  $E, E' \in \mathcal{E}$  it holds that

$$D_{\alpha}\left(\mathcal{M}(E) \parallel \mathcal{M}(E')\right) \leq \rho$$

In this work, we call two datasets E, E' to be adjacent if  $E' = E \cup \{x\}$  (or vice versa).

**Definition A.3** (Sampled Gaussian Mechanism (SGM) [1, 30]). Let f be an arbitrary function mapping subsets of  $\mathcal{E}$  to  $\mathbb{R}^d$ . We define the Sampled Gaussian mechanism (SGM) parametrized with the sampling rate  $0 < q \le 1$  and the noise  $\sigma > 0$  as

$$SG_{q,\sigma} \stackrel{\Delta}{=} f(\{ \boldsymbol{x} : \boldsymbol{x} \in E \text{ is sampled with probability } q \}) + \mathcal{N}(0, \sigma^2 \mathbb{I}_d),$$

where each element of E is independently and randomly sampled with probability q without replacement.

The sampled Gaussian mechanism consists of adding i.i.d Gaussian noise with zero mean and variance  $\sigma^2$  to each coordinate of the true output of f. In fact, the sampled Gaussian mechanism draws random vector values from a multivariate isotropic Gaussian distribution denoted by  $\mathcal{N}(0, \sigma^2 \mathbb{I}_d)$ , where d is omitted if it is unambiguous in the given context.

# A.2 Analysis

The privacy analysis of Fed-GLOSS-DP and other DP baselines follows the analysis framework used for gradient-based record level-DP methods in FL []. In this framework, each individual local update is performed as a single SGM (Definition A.3) that involves clipping the per-example gradients on a local batch and subsequently adding Gaussian noise to the averaged batch gradient (Algorithm 2). The privacy cost accumulated over multiple local updates and global rounds is then quantified utilizing the revisited moment accountant [30], which presents an adapted version of the moments accountant introduced in Abadi et al. [1] by adapting to the notion of RDP (Definition A.2). Finally, to obtain interpretable results and enable transparent comparisons to established approaches, we convert the privacy cost from  $(\alpha, \rho)$ -RDP to  $(\varepsilon, \delta)$ -DP by employing Theorem A.6 provided by [2].

Let  $\mu_0$  denote the pdf of  $\mathcal{N}(0, \sigma^2)$  and let  $\mu_1$  denote the pdf of  $\mathcal{N}(1, \sigma^2)$ . Let  $\mu$  be the mixture of two Gaussians  $\mu = (1 - q)\mu_0 + a\mu_1$ , where q is the sampling probability of a single record in a single round.

**Theorem A.4.** [30]. Let  $SG_{q,\sigma}$  be the Sampled Gaussian mechanism for some function f and under the assumption  $\Delta_2 f \leq 1$  for any adjacent  $E, E' \in \mathcal{E}$ . Then  $SG_{q,\sigma}$  satisfies  $(\alpha, \rho)$ -RDP if

$$\rho \le \frac{1}{\alpha - 1} \log \left( \max\{A_{\alpha}, B_{\alpha}\} \right) \tag{17}$$

where  $A_{\alpha} \stackrel{\Delta}{=} \mathbb{E}_{z \sim \mu_0}[(\mu(z)/\mu_0(z))]$  and  $B_{\alpha} \stackrel{\Delta}{=} \mathbb{E}_{z \sim \mu}[(\mu_0(z)/\mu(z))]$ 

Theorem A.4 states that applying SGM to a function of sensitivity (Eq. 7) at most 1 (which also holds for larger values without loss of generality) satisfies  $(\alpha, \rho)$ -RDP if  $\rho \leq \frac{1}{\alpha - 1} \log(\max\{A_{\alpha}, B_{\alpha}\})$ . Thus, analyzing RDP properties of SGM is equivalent to upper bounding  $A_{\alpha}$  and  $B_{\alpha}$ .

From Corollary 7 in Mironov et al. [30],  $A_{\alpha} \geq B_{\alpha}$  for any  $\alpha \geq 1$ . Therefore, we can reformulate 17 as

$$\rho \le \xi_{\mathcal{N}}(\alpha|q) = \frac{1}{\alpha - 1} \log A_{\alpha} \tag{18}$$

To compute  $A_{\alpha}$ , we use the numerically stable computation approach proposed in Section 3.3 of Mironov et al. [30]. The specific approach used depends on whether  $\alpha$  is expressed as an integer or a fractional value.

**Theorem A.5** (Composability [29]). Suppose that a mechanism  $\mathcal{M}$  consists of a sequence of adaptive mechanisms  $\mathcal{M}_1, \ldots, \mathcal{M}_k$  where  $\mathcal{M}_i : \prod_{j=1}^{i-1} \mathcal{R}_j \times \mathcal{E} \to \mathcal{R}_i$ . If all mechanisms in the sequence are  $(\alpha, \rho)$ -RDP, then the composition of the sequence is  $(\alpha, k\rho)$ -RDP.

In particular, Theorem A.5 holds when the mechanisms themselves are chosen based on the (public) output of the previous mechanisms. By Theorem A.5, it suffices to compute  $\xi_{\mathcal{N}}(\alpha|q)$  at each step and sum them up to bound the overall RDP privacy budget of an iterative mechanism composed of single DP mechanisms at each step.

**Theorem A.6** (Conversion from RDP to DP [2]). *If a mechanism*  $\mathcal{M}$  *is*  $(\alpha, \rho)$ -RDP then it is  $((\rho + \log((\alpha - 1)/\alpha) - (\log \delta + \log \alpha)/(\alpha - 1), \delta)$ -DP for any  $0 < \delta < 1$ .

**Theorem A.7** (Privacy of Fed-GLOSS-DP). For any  $0 < \delta < 1$  and  $\alpha \ge 1$ , Fed-GLOSS-DP is  $(\varepsilon, \delta)$ -DP, with

$$\varepsilon = \min_{\alpha} \left( M \cdot \xi_{\mathcal{N}}(\alpha|q_1) + M(T-1) \cdot \xi_{\mathcal{N}}(\alpha|q_2) + \log((\alpha-1)/\alpha) - (\log \delta + \log \alpha)/(\alpha-1) \right)$$
(19)

Here,  $\xi_{\mathcal{N}}(\alpha|q)$  is defined in Eq. 18,  $q_1 = \frac{C \cdot \mathbb{B}}{\min_k |\mathcal{D}_k|}$ ,  $q_2 = \frac{\mathbb{B}}{\min_k |\mathcal{D}_k|}$ , M is the number of federated rounds, T is the total number of local updates (i.e., total accesses to local private data) per federated round, C is the probability of selecting any client per federated round,  $\mathbb{B}$  is the local batch size, and  $|\mathcal{D}_k|$  denotes the local dataset size.

The proof follows from Theorems A.4, A.5,A.6 and the fact that a record is sampled in the very first SGD iteration of every round if two conditions are met. First, the corresponding client must be selected, which occurs with a probability of C. Second, the locally sampled batch at that client must contain the record, which has a probability of at most  $\frac{\mathbb{B}}{\min_k |\mathcal{D}_k|}$ . However, the adaptive composition of consecutive SGD iterations are considered where the output of a single iteration depends on the output of the previous iterations. Therefore, the sampling probability for the first batch is  $q_1 = \frac{C \cdot \mathbb{B}}{\min_k |\mathcal{D}_k|}$ , while the sampling probability for every subsequent SGD iteration within the same round is at most  $q_2 = \frac{\mathbb{B}}{\min_k |\mathcal{D}_k|}$  conditioned on the result of the first iteration.

#### **B** Algorithms

**Distance metric** Following existing works [42, 43], the distance  $\mathcal{L}_{dis}$  (in Equation 11 and 12 of the main paper) between the real and synthetic gradients is defined to be the sum of the cosine distance at each layer. Let  $\mathbf{w}^{(l)}$  denote the weight at the l-th layer, the distance can be formularized as:

$$\mathcal{L}_{dis}\Big(\nabla_{\mathbf{w}}\mathcal{L}(\mathbf{w}, \mathcal{D}_k), \nabla_{\mathbf{w}}\mathcal{L}(\mathbf{w}, \mathcal{S}_k)\Big)$$
(20)

$$= \sum_{l=1}^{L} d\left(\nabla_{\mathbf{w}^{(l)}} \mathcal{L}(\mathbf{w}^{(l)}, \mathcal{D}_k), \nabla_{\mathbf{w}^{(l)}} \mathcal{L}(\mathbf{w}^{(l)}, \mathcal{S}_k)\right) + \|\nabla_{\mathbf{w}^{(l)}} \mathcal{L}(\mathbf{w}^{(l)}, \mathcal{D}_k) - \nabla_{\mathbf{w}^{(l)}} \mathcal{L}(\mathbf{w}^{(l)}, \mathcal{S}_k)\|_{2}^{2}$$
(21)

d denotes the cosine distance between the gradients at each layer:

$$d(\boldsymbol{A}, \boldsymbol{B}) = \sum_{i=1}^{out} \left( 1 - \frac{\boldsymbol{A}_{i\cdot} \cdot \boldsymbol{B}_{i\cdot}}{\|\boldsymbol{A}_{i\cdot}\| \|\boldsymbol{B}_{i\cdot}\|} \right)$$

where  $A_i$  and  $B_i$  represent the flattened gradient vectors corresponding to each output node i. In FC layers,  $\theta^l$  is a 2D tensor with dimension  $out \times in$  and the flattened gradient vector has dimension in, while in Conv layers,  $\theta^l$  is a 4D tensor with dimensionality  $out \times in \times h \times w$  and the flattened vector has dimension  $in \times h \times w$ . Here we use out, in, in, in, in to denote the number of output and input channels, kernel height, and width, respectively.

**Fed-GLOSS-DP** We present the pseudocode of the Fed-GLOSS with record-level DP in Algorithm 2, which is supplementary to Sec. 4.4 of the main paper.

# Algorithm 2 Fed-GLOSS-DP function ServerExecute: **Initialize** global weight $\mathbf{w}_g^{1,1}$ , Fix the radius r/\* Local approximation \*/ for $m=1,\ldots,M$ do for $k = 1, \ldots, K$ do $S_k \leftarrow \text{ClientsExecute}(k, r, \mathbf{w}_q^{m,1})$ /\* Global optimization \*/ $t \leftarrow 1$ $\begin{aligned} & \textbf{while} \ \|\mathbf{w}_g^{m,1} - \mathbf{w}_g^{m,t}\| < r \ \textbf{do} \\ & \mathbf{w}_g^{m,t+1} = \mathbf{w}_g^{m,t} - \sum_{k=1}^K \eta \frac{1}{K} \nabla_{\mathbf{w}} \mathcal{L}(\mathbf{w}_g^{m,t}, \mathcal{S}_k) \\ & t \leftarrow t+1 \end{aligned}$ end while $\mathbf{w}_{a}^{m+1,1} \leftarrow \mathbf{w}_{a}^{m,t}$ end for **Return:** global model weight $\mathbf{w}_g^{M+1,1}$ **function** ClientExecute $(k, r, \mathbf{w}_q^{m,1})$ : **Initialize** $S_k$ : $\{\hat{x}_k^m\}$ from Gaussian noise or $\{\hat{x}_k^{m-1}\}$ , $\{\hat{y}_k\}$ to be a balanced set for $i=1,\ldots,R_i$ do /\* Resample training trajectories \*/ Reset $t \leftarrow 1$ and model $\mathbf{w}_k^{m,1} \leftarrow \mathbf{w}_g^{m,1}$ while $||\mathbf{w}_k^{m,t} - \mathbf{w}_k^{m,1}|| < r \mathbf{do}$ Uniformly sample random batch $\{(\boldsymbol{x}_k^i, y_k^i)\}_{i=1}^{\mathbb{B}}$ from $\mathcal{D}_k$ for each $(\boldsymbol{x}_k^i, y_k^i)$ do /\* Compute per-example gradients on client data \*/ $g^{\mathcal{D}}(\boldsymbol{x}_k^i) = \nabla_{\mathbf{w}} \ell(\mathbf{w}_k^{m,t}, \boldsymbol{x}_k^i, y_k^i)$ /\* Clip gradients with bound $\mathbb{C}$ \*/ $\widetilde{g^{\mathcal{D}}}(\boldsymbol{x}_k^i) = g^{\mathcal{D}}(\boldsymbol{x}_k^i) \cdot \min(1, \mathbb{C}/\|g^{\mathcal{D}}(\boldsymbol{x}_k^i)\|_2)$ end for /\* Add noise to average gradient by Gaussian mechanism \*/ Compute $\nabla \widetilde{\mathcal{L}}(\mathbf{w}_k^{m,t}, \mathcal{D}_k) = \frac{1}{\mathbb{B}} \sum_{i=1}^{\mathbb{B}} (\widetilde{g^{\mathcal{D}}}(\mathbf{x}_k^i) + \mathcal{N}(0, \sigma^2 \mathbb{C}^2 I))$ for $j = 1, \dots, R_b$ do /\* Update synthetic set $\mathcal{S}_k$ \*/ $S_k = S_k - \tau \nabla_{S_k} \mathcal{L}_{dis} \left( \nabla \widetilde{\mathcal{L}}(\mathbf{w}_k^{m,t}, \mathcal{D}_k), \nabla \mathcal{L}(\mathbf{w}_k^{m,t}, \mathcal{S}_k) \right)$ end for for $l=1,\ldots,R_l$ do /\* Update local model parameter $\mathbf{w}_k$ \*/ $\mathbf{w}_k^{m,t+1} = \mathbf{w}_k^{m,t} - \eta \nabla \mathcal{L}(\mathbf{w}_k^{m,t}, \mathcal{S}_k)$ end for end while end for

**Return:** Synthetic set  $S_k$ 

# C Setup Details

We consider a standard classification task by training federated ConvNets [20] on three benchmark datasets: MNIST [19], FashionMNIST [38], and CIFAR-10 [17]. Our study focuses on the non-IID setting where five clients possess disjoint class sets, meaning each client holds two unique classes. This scenario is typically considered challenging [11] and mirrors the cross-silo setting [12] where all clients participate in every training round while maintaining a relatively large amount of data, yet exhibiting statistical divergence (e.g., envision the practical scenario for collaborations among hospitals).

By default, we set the hyperparameters  $(R_i, R_l, R_b, r)$  to be (4, 2, 10, 1.5) and (1, 0, 5, 10, 0.1) for DP (Differential Privacy) and non-DP training, respectively. Additionally, we include a weight of 0.1 for Mean Squared Error (MSE) regularization in our method (Eq. 12 and 21. To avoid infinite loops caused by neighborhood search, we limit the iterations in Algorithm 1 (referred to as Algorithm 1 in the original text) to a maximum of 5.

Our method utilizes a learning rate of 100 for updating synthetic images, and we specify the learning schedulers as described below. For training the baselines, we adhere to the FL (Federated Learning) benchmarks [27, 33] and use the official codes. All experiments are conducted on a single Titan RTX GPU and repeated three times with different random seeds. Further implementation details are provided in the following sections. The source code will be made publicly available upon publication.

#### C.1 Architectures

We provide the details of the federated ConvNet used in our paper. The network consists of three convolutional layers, followed by two fully-connected layers. ReLU activation functions are applied between each layer. Each convolution layer, except for the input layer, is composed of 128 (input channels) and 128 (output channels) with  $3 \times 3$  filters. Following prior work [35, 33, 41, 4], we attach Group Normalization [37] before the activation functions to stabilize training. For classification, the network utilizes a global average pooling layer to extract features, which are then fed into the final classification layer for prediction. The entire network contains a total of 317,706 floating-point parameters. The model details are listed below.

```
ConvNet(
    (features): Sequential(
        (0): Conv2d(3, 128, kernel_size=(3, 3), stride=(1, 1), padding=(1, 1))
        (1): GroupNorm(128, 128, eps=le-05, affine=True)
        (2): ReLU(inplace=True)
        (3): AvgPool2d(kernel_size=2, stride=2, padding=0)
        (4): Conv2d(128, 128, kernel_size=(3, 3), stride=(1, 1), padding=(1, 1))
        (5): GroupNorm(128, 128, eps=le-05, affine=True)
        (6): ReLU(inplace=True)
        (7): AvgPool2d(kernel_size=2, stride=2, padding=0)
        (8): Conv2d(128, 128, kernel_size=(3, 3), stride=(1, 1), padding=(1, 1))
        (9): GroupNorm(128, 128, eps=le-05, affine=True)
        (10): ReLU(inplace=True)
        (11): AvgPool2d(kernel_size=2, stride=2, padding=0)
    )
    (classifier): Linear(in_features=2048, out_features=10, bias=True)
```

# C.2 Non-DP

We maintain a consistent total of 60 communication rounds for MNIST and FashionMNIST, and 200 rounds for CIFAR-10. Following prior work [27, 33], we tune the hyper-parameters for various gradient-sharing schemes, including FedSGD [27], FedAvg [27], FedProx [23], and SCAFFOLD [13]. We use a client learning rate of 0.01 for MNIST and FashionMNIST and 0.1 for CIFAR-10. All baselines are equipped with a fixed server learning rate of 1 and a cosine learning rate decay for the clients (potentially diverge, if without decay [33]). While hyper-parameter searching is an active field and requires non-trivial effort [16], we explore a proper number of local epochs by running FedAvg for 200 rounds with  $\{1,3,5\}$  local epochs, leading to 69.13, 69.39, and 71.91, respectively. This suggests that 5 local epochs work best for FedAvg. We also set 5 local epochs for the rest of baselines

	DP-FedAvg (low)	DP-FedAvg (high)	Ours	DP-FedAvg (low)	DP-FedAvg (high)	Ours
ε		2.79			10.18	
MNIST	16.25	45.25	60.72	51.53	86.99	87.77
FashionMNIST	13.39	50.11	59.85	59.26	72.78	73.00
CIFAR-10	9.37	17.11	21.42	16.16	31.15	36.09

Table 4: Comparison of DP-FedAvg with different learning rates: 0.1 (DP-FedAvg high) and 0.002 (DP-FedAvg low). We use the same initial learning rate as our method (0.002) for DP-FedAvg (low).

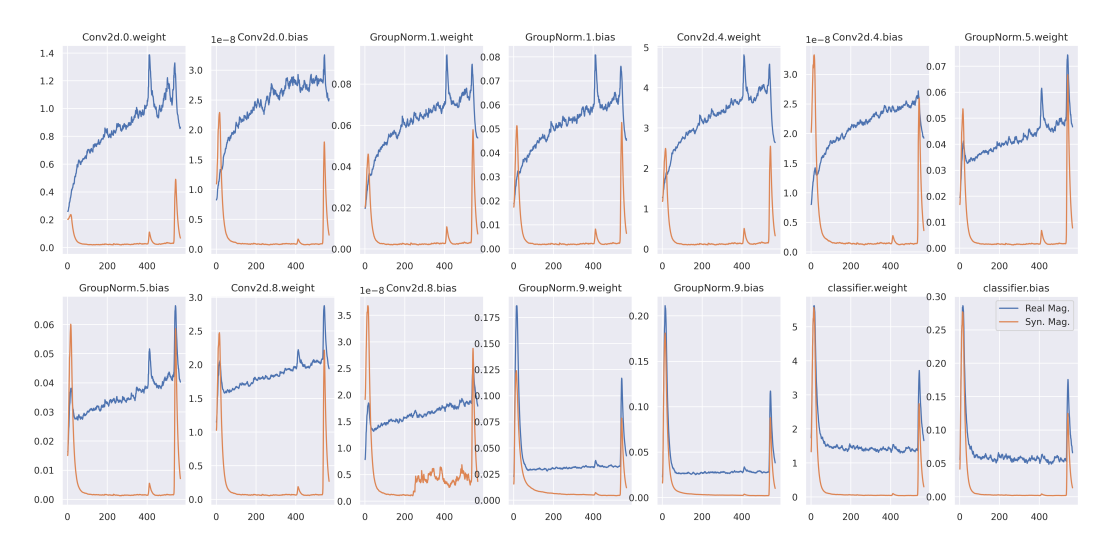


Figure 8: Discrepancy in gradient magnitudes between real and synthetic data. The noticeable difference in magnitudes during training highlights the limitation of solely regulating gradient directions, as optimizing without magnitude information introduces training instability.

for a fair comparison regarding data exploitation and communication efficiency. For FedProx, we assign a weight of 0.1 for the proximal regularization term.

In the case of Fed-GLOSS, we use a server learning rate of 0.01 for MNIST and FashionMNIST, and 0.1 for CIFAR-10. These learning rates match the client learning rates used in the gradient-sharing baselines, while shifting the potentially biased local optimization to the server side. Additionally, our method adopts the same cosine learning rate decay as the baselines. These settings ensure a fair comparison as the parameters are not biased in favor of our method in non-private settings. Furthermore, in each communication round, we assign 50 images to each class and re-initialize the synthetic images from scratch. After receiving the images, the server performs full gradient descent to update the model parameters. This process ensures that the model is updated based on the collective knowledge obtained from the synthetic images generated by the clients.

# C.3 DP

In this experiment, we compare the performance of Fed-GLOSS-DP to DP-FedAvg and DP-FedProx. We set a learning rate of 0.1 with cosine decay for the baselines. Following the approach of Kurakin et al. [18], we initially verify that the learning rate works well in non-private settings. Then, we search for the sensitivity value from a grid of 1.0, 0.5, 0.2, 0.1. This results in a sensitivity of 0.1 for DP-FedAvg, 0.2 for DP-FedProx, and 1.0 for Fed-GLOSS-DP. Moreover, our method assigns 10 images to each class to mitigate the negative impact of differential privacy (DP) noise and a lower learning rate of 0.002, coupled with cosine decay, for all DP experiments.

# D Additional Analysis

#### **D.1** Matching Criteria

We analyze our design choices by using our method to fit gradients computed on a single batch. We simplify the learning task by employing only one client that contains all training data, resembling centralized training or FedSGD with a single client. In this setup, the client immediately communicates the gradients to the central server after computing them on a single batch. This scenario can be seen as a trivial federated learning task, as it does not involve any model drifting (non-IID) or communication budget constraints. It is worth noting that the baseline performance in this setting is an *ideal* case that does not apply in any practical FL use cases (or out of scope of federated learning).

Gradient Magnitudes While previous research [43, 40, 9] suggests that gradient directions are more crucial than magnitudes (Eq. B), our study demonstrates that as training progresses, the magnitudes of synthetic gradients (i.e., gradients obtained from synthetic images) can differ significantly from real gradients. In Fig. 8, we display the gradient magnitudes of each layer in a ConvNet. Our findings indicate that even with only 500 iterations, the magnitudes of synthetic gradients (orange) noticeably deviate from the real ones (blue), causing unnecessary instability during training.

**Post-hoc Magnitude Calibration** To further validate the issue, we implement a post-hoc magnitude calibration, called *Calibration* in Fig. 9. It calibrates the gradients obtained from the synthetic images on the server. Specifically, the clients send the layer-wise magnitudes of real

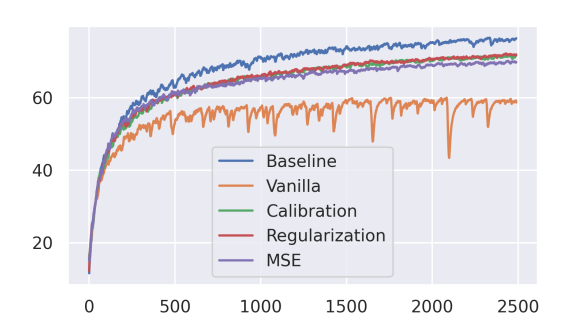


Figure 9: Performance comparison of fitting one batch. **Baseline**: FedSGD with one client. **Vanilla**: our method with cosine similarity. **Calibration**: our method with cosine similarity and magnitude calibration. **Regularization**: our method with cosine similarity and MSE regularization. **MSE**: our method with an MSE loss.

gradients  $\|\nabla_{\mathbf{w}} \mathcal{L}(\mathbf{w}, \mathcal{D}_k)\|$  to the server, followed by a transformation on the server:

$$\frac{\nabla_{\mathbf{w}} \mathcal{L}(\mathbf{w}, \mathcal{S}_k)}{\|\nabla_{\mathbf{w}} \mathcal{L}(\mathbf{w}, \mathcal{S}_k)\|} \|\nabla_{\mathbf{w}} \mathcal{L}(\mathbf{w}, \mathcal{D}_k)\|. \tag{22}$$

In Fig. 9, We observe that the synthetic images with the magnitude calibration successfully and continuously improve over the one without the calibration (Vanilla). It implies that even with the same cosine similarity, inaccurate gradient magnitudes could dramatically fail the training. It is worth noting that the performance gap between the baseline and our method in this experiment does not apply to federated learning since FL models suffer from non-IID problems induced by multiple steps and clients, the gradient-sharing schemes, such as FedAvg, overly approximate the update signal, further enhancing the problem. Meanwhile, it also suggests an opportunity to improve our method if future work can further bridge the gap.

Mean Square Error (MSE) Regularization Although calibration can improve performance, it is not suitable for federated learning due to two reasons. Firstly, when the synthetic images  $S_k$  from different clients are merged into a dataset for server optimization, it remains unclear how to apply Eq. 22 to the averaged gradients of the merged dataset S, especially when multiple-step optimization is involved. Secondly, transmitting magnitudes can pose privacy risks. Instead of explicit calibration, we propose using MSE regularization (Eq. B) to limit potential magnitude deviations while focusing on the directions. As depicted in Fig. 9, our proposed method remains close to the calibration method, suggesting that regularization prevents mismatch. Moreover, we present that MSE improves over the vanilla method but still falls behind *Calibration* and *Regularization*.

# **D.2** Radius Selection

In Sec. 5.4, we show that the effective approximation regions change across rounds. A fixed predefined training iterations may cause sub-optimal performance. To complement the experiments, we additionally plot the corresponding training iterations on the server side in Fig. 10. We observed that *Max* and *Median* tend to be more aggressive by updating for more epochs, granting faster improvement, while *Min* optimizes more conservatively. Interestingly, we found that all three

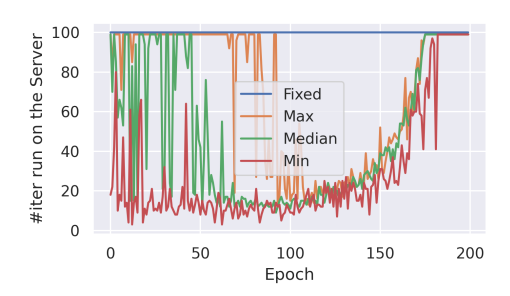


Figure 10: Training iterations for different radius selection strategies.

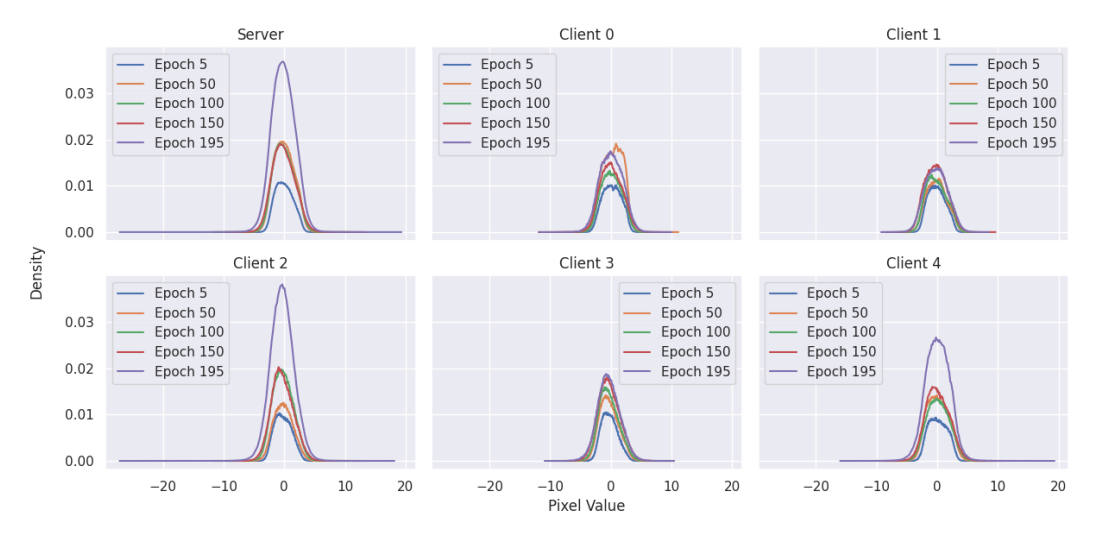


Figure 11: Pixel distributions in non-private settings. The plot illustrates the evolution of pixel values in synthetic images during training. At the early training stage, the pixel range is wider and gradually concentrates around zero as the model approaches convergence, implying that the synthetic images reflects the training status.

proposed strategies exhibit similar behavior in the later stages of training, which is in stark contrast to the fixed strategy.

#### **D.3** Qualitative Results

In this section, we examine the synthetic images and analyze the distribution of pixel values. In non-private settings, Fig. 11 displays the pixel value distributions of all synthetic images at epochs 5, 50, 100, 150, and 195, both on the server and the clients. We made several observations from these visualizations. Firstly, within the same round, the distributions of pixel values on each client exhibit distinct behavior, indicating the diversity of private data statistics across clients. Secondly, the distributions also vary across different epochs. At earlier stages, the synthetic images present a wider range of values, gradually concentrating around zero as training progresses. This phenomenon introduces more detailed information for training and demonstrates that our method faithfully reflects the training status of each client. To provide a more detailed analysis, we include histograms of pixel value distributions at different epochs in Fig. 14. Furthermore, Fig. 12 showcases visual examples of the synthetic images corresponding to the labels "airplane," "automobile," "bird," and "cat." These visualizations illustrate that the images from earlier epochs contain larger pixel values and gradually incorporate more noise as the training progresses, thus implementing details of gradients.

On the other hand, Fed-GLOSS-DP integrates DP to sanitize gradients and secure privacy. Fig. 15 illustrates that the pixel distributions are more similar across clients in the DP setting. This observation confirms the effectiveness of our method in preserving privacy and makes it more challenging to



Figure 12: Visualization of synthetic images at epochs 5, 50, and 196 in non-private settings. The first row presents the images with the pixel values clipped to the range [0, 1]. The second row shows the same images as the first row but with values normalized by subtracting the minimum value and dividing it by the range between the maximum and minimum values. The four rows in a set correspond to airplane, automobile, bird, and cat, respectively.

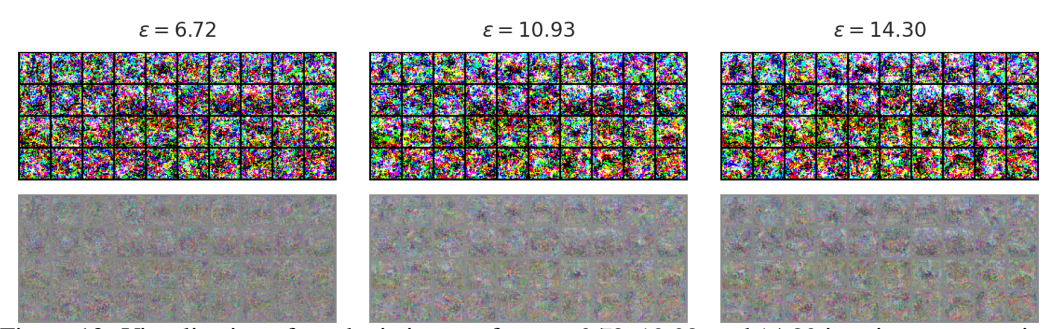


Figure 13: Visualization of synthetic images for  $\varepsilon=6.72,\,10.93,\,$  and 14.30 in privacy-preserving settings. The first row presents the images with the pixel values clipped to the range [0,1]. The second row shows the same images as the first row but with values normalized by subtracting the minimum value and dividing it by the range between the maximum and minimum values. The four rows in a set correspond to airplane, automobile, bird, and cat, respectively.

extract sensitive information from these distributions, as compared to the non-private settings depicted in Fig. 14. To further validate the privacy protection achieved by Fed-GLOSS-DP, we provide a visualization in Fig. 13. The images generated in the DP setting appear like noise and convey minimal information through visual appearance, thus ensuring a high level of privacy preservation.

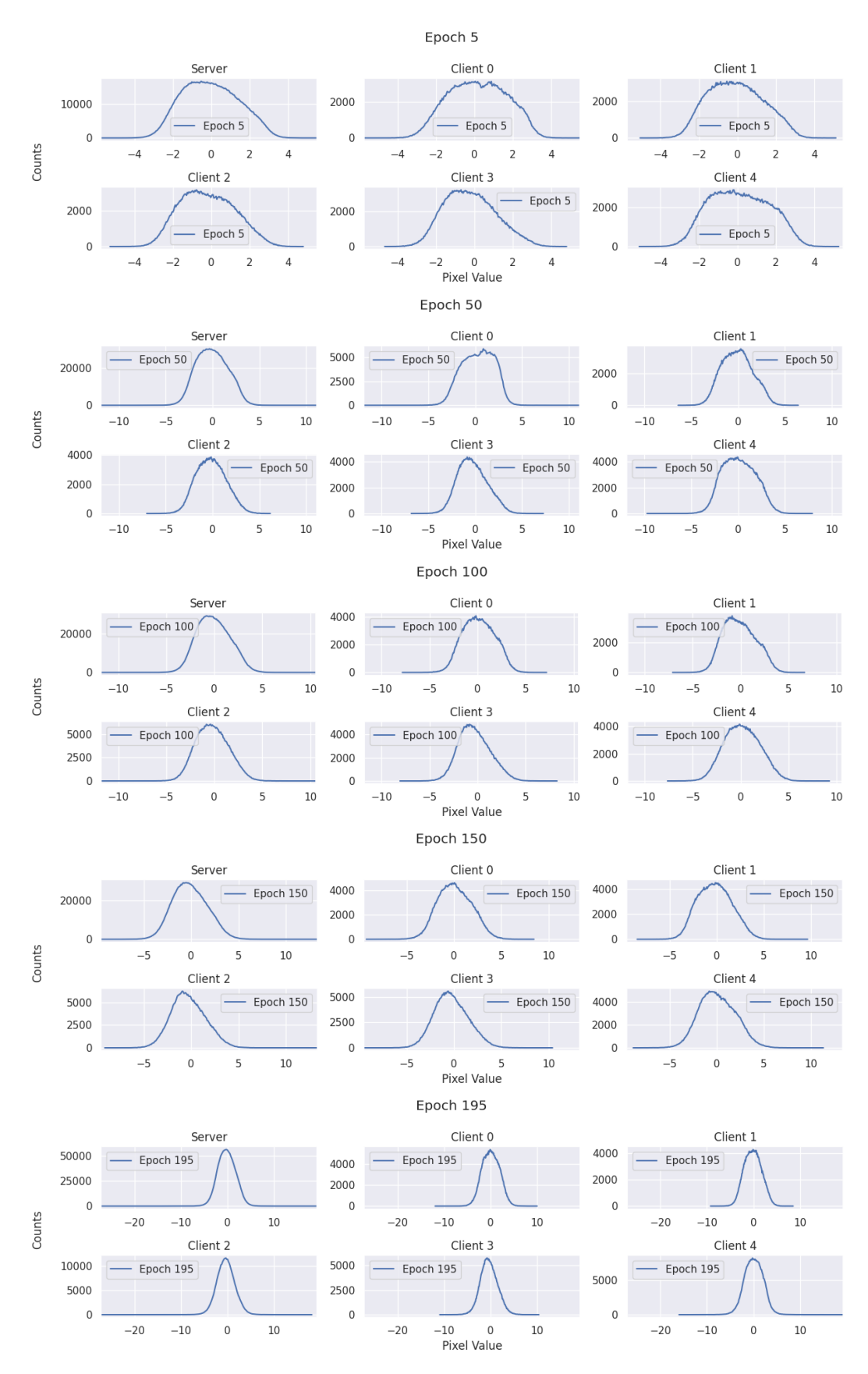


Figure 14: Pixel distributions at epochs 5, 50, 100, 150, and 195 in non-private settings.

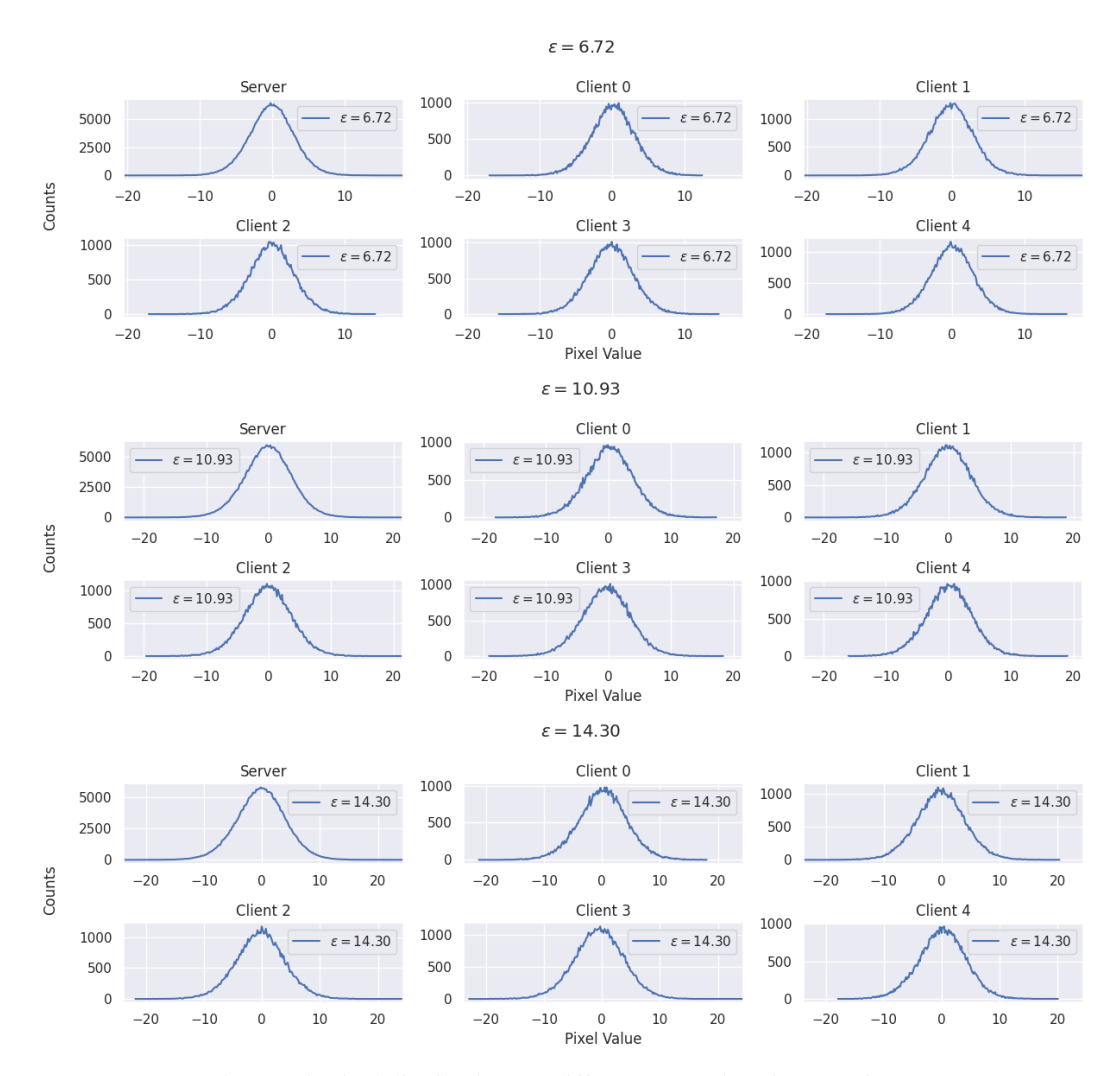


Figure 15: Pixel distributions at different stages in private settings.